WATER RESOURCES RESEARCH, VOL. 46, W05501, doi:10.1029/2009WR007720, 2010

Measurement and simulation of the effect of compaction on the pore structure and saturated hydraulic conductivity of grassland and arable soil

G. P. Matthews,[1] G. M. Laudone,[1] A. S. Gregory,[2] N. R. A. Bird,[2] A. G. de G. Matthews,[3] and W. R. Whalley[2]

Received 8 January 2009; revised 31 August 2009; accepted 4 November 2009; published 1 May 2010.

[1] Measurements have been made of the effect of compaction on water retention, saturated hydraulic conductivity, and porosity of two English soils: North Wyke (NW) grassland clay topsoil and Broadbalk silty topsoil, fertilized inorganically (PKMg) or with farmyard manure (FYM). As expected, the FYM topsoil had greater porosity and greater water retention than PKMg topsoil, and the NW clay topsoil retained more water at each matric potential than the silty topsoils. Compaction had a clear effect on water retention at matric potentials wetter than −10 kPa for the PKMg and FYM soils, corresponding to voids greater than 30 μm cylindrical diameter, whereas smaller voids appeared to be unaffected. The Pore-Cor void network model has been improved by including a Euler beta distribution to describe the sizes of the narrow interconnections, termed throats. The model revealed a change from bimodal to unimodal throat size distributions on compaction, as well as a reduction in sizes overall. It also matched the water retention curves more closely than van Genuchten fits and correctly predicted changes in saturated hydraulic conductivity better than those predicted by a prior statistical approach. However, the changes in hydraulic conductivity were masked by the stochastic variability of the model. Also, an artifact of the model, namely its inability to pack small features close together, caused incorrect increases in pore sizes on compaction. These deficiencies in the model demonstrate the need for an explicitly dual porous network model to account for the effects of compaction in soil.

Citation: Matthews, G. P., G. M. Laudone, A. S. Gregory, N. R. A. Bird, A. G. de G. Matthews, and W. R. Whalley (2010), Measurement and simulation of the effect of compaction on the pore structure and saturated hydraulic conductivity of grassland and arable soil, *Water Resour. Res.*, *46*, W05501, doi:10.1029/2009WR007720.

1. Introduction

1.1. Difficulties of the Traditional Approach

[2] We have investigated the extent to which the pore sizes within soil samples can be inferred from water retention curves, and the extent to which saturated hydraulic conductivities can be related to these pore size distributions and hence to the water retention curves. Specifically, the effects of soil compaction have been explored. These relationships have been studied for many decades by soil physicists. The traditional approach has tended to involve the parameterization of a water retention curve into a tractable mathematical form dependent on two or three fitting parameters, and then the seeking of a relationship between these parameters and the saturated or unsaturated hydraulic conductivity. This approach suffers three fundamental disadvantages. First, water retention curves are difficult to measure, so are typically determined at only a few tensions, thus leaving very few statistical degrees of freedom for a fitting curve. Once reliable experimental results are achieved, the next problem is that the functional form of the smoothing curve may be too restrictive, and may not accurately reflect the subtle features of the water retention curve. Finally, the fitting parameters themselves are primarily designed for reliability of fitting rather than being directly connected to the soil structure, so inferring structural information from them is often difficult.

[3] The present study is designed to address these issues for samples of grassland and arable soil, including different arable soil treatments, at different levels of compaction. It employs water retention curves measured at many tensions with high accuracy. Rather than fitting mathematical functions to the water retention curves, we generate void networks which closely match the experimental porosity and percolation characteristics. We review how well the geometrically constrained void networks reveal characteristics of the soil samples and the effect of compaction, and the extent to which a network model approach can predict saturated hydraulic conductivity. We compare the predictions to saturated hydraulic conductivities generated by a statistical approach originating with *Childs and Collis-George* [1950].

[1]School of Geography, Earth and Environmental Sciences, University of Plymouth, Devon, UK.
[2]Department of Soil Science, Rothamsted Research, Harpenden, UK.
[3]Cavendish Laboratory, University of Cambridge, Cambridge, UK.

0043-1397/10/2009WR007720

1.2. Recent Background

[4] Perhaps the most basic parameterization of water retention curves is the Campbell model which assumes:

$$\psi/\psi_e = (\theta/\theta_s)^{-b} \quad (1)$$

where ψ is the matric potential, ψ_e is the air entry matric potential, θ is the volumetric soil water content, θ_s is the volumetric soil water content at saturation, and b a fitting parameter. It has been combined with the Gardner model, which assumes that the relative hydraulic conductivity is proportional to the exponential of soil water matric potential:

$$K/K_s = \exp(A\psi) \quad (2)$$

where K is the hydraulic conductivity, K_s the saturated hydraulic conductivity and A is a fitting parameter related to the macroscopic capillary length of the soil [*Kawamoto et al.*, 2006]. The combined equations have been fitted to three distinct regions of the water retention curve by *Poulsen et al.* [2002]. A double exponential fit has recently been made, with the proposal that the two exponential terms relate to the matrix and structural pore spaces in the soil [*Dexter et al.*, 2008]. Another approach is to assume that the void sizes follow a lognormal distribution [*Kosugi*, 1999], but that can be difficult to justify in a substance as complicated as soil.

[5] A much more popular approach is to fit the van Genuchten equation, although there can be problems in its use near saturation [*Schaap and van Genuchten*, 2005]. *Stange and Horn* [2005] have expressed the effect of compaction in terms of adjustable van Genuchten coefficients. The van Genuchten equation is frequently combined with a Mualem approach to predict unsaturated hydraulic conductivity. Also popular is the Brooks-Corey model [*Neuweiler and Cirpka*, 2005], often as modified by Jarvis [*Borgesen et al.*, 2006]. Although invaluable for such purposes as pedo transfer functions, workers have recognized the difficulty of interpreting van Genuchten and Brooks-Corey parameters with respect to the structure of the soil.

[6] In this work, we measure the effect of compaction on saturated hydraulic conductivity K_s only. However, there is also an extensive literature on the effect of compaction on unsaturated hydraulic conductivity K. Of interest is that *Richard et al.* [2001] found that at tensions lower than (drier than) −15 kPa, K was actually greater in compacted soil than uncompacted soil. They ascribe this to the presence in compacted soils of a greater continuity of saturated pores through a denser matrix of aggregates, as later stated by *Berli et al.* [2008]. They also describe the creation of "relict" structural pores within a textural matrix in compacted soils which act as reservoirs that may only be drained once the smaller pore throat is drained.

[7] Studies of soil compaction confirm that the ease of compaction depends crucially on the water content [*Tarawally et al.*, 2004]; compaction of drier nonplastic granular tills results in a more uniform ultimate pore size distribution than compaction of a wetter soil [*Davoudi and Lefebvre*, 2005], while in Chinese Ultisols the precompression stress decreases exponentially with increasing soil water content [*Peng et al.*, 2004]. For sandy soils, measurement of residual water content is crucial in being able to predict the saturated and field water contents under compaction [*Oliver and Smettem*, 2005]. A greater number of macropores above 50 μm have been observed in arable relative to grassland soils [*Alaoui and Goetz*, 2008]. The destruction of macropores is observable in pronounced changes in the wet ends of water retention curves, whereas micropores are relatively unaffected [*Zhang et al.*, 2006]. Although natural macropores are sensitive to compaction, artificial macropores are relatively robust [*Schaffer et al.*, 2008]. Measurement of shrinkage is vital when studying compaction, and indeed the use of soil shrinkage curves has been proposed as method of characterizing changes in macroporosity and microporosity [*Boivin et al.*, 2006].

[8] Bromide tracers reveal double concentration peaks caused by the shadow effects of compacted soil clods [*Coquet et al.*, 2005]. Dye tracer experiments show a destruction of more tortuous macropores by compaction, as inferred by the reduction in lateral exchange from macropores into the soil matrix [*Alaoui and Goetz*, 2008]. In sandy loams, compaction leads to an increased likelihood of preferential flow, whereas in clay soils, preferential flow occurs except at high compaction [*Mooney and Nipattasuk*, 2003].

[9] With regard to the use of void network models in relating water retention curves to void sizes and hydraulic conductivities, *van Dijke and Piri* [2007] comment that the goals have changed little in the last 60 years. A particular problem with applying such models to soil is the simplicity of a network of, for example, pores connected by cylindrical "throats" relative to the extreme complexity of the structure of soil. However, the complexity and capability of such models are now being enhanced by the availability of much greater computing power. The network model used in this work, named Pore-Cor, has had some success in modeling trends in soil texture [*Peat et al.*, 2000], trends with depth [*Johnson et al.*, 2003] and the structuring of soil under clover [*Holtham et al.*, 2007]. However, two obvious weaknesses of this model are the restriction of the throat size distribution to a log linear functional form, and the equispacing of the void features in Cartesian coordinates without regard to their size. In this work, we remove one of these limitations by replacing the log linear distribution with a highly flexible Euler beta distribution, as also previously used in less flexible form by *Or and Tuller* [1999].

2. Modeling

2.1. Theory

[10] Three-dimensional void networks are generated by stochastically creating unit cells comprising an array of 1000 (10 × 10 × 10) cubic pores connected by up to 3000 cylindrical throats (see Figure 1). The unit cells are connected together and have periodic boundary conditions; that is, fluid moving out from one side of a unit cell flows into the adjacent side of its neighboring replicate. Figure 1 shows two unit cells connected together in each direction; that is, 8 unit cells in a 2 × 2 × 2 array. Fluids are injected through the xy plane at maximum z in the $-z$ direction. The geometries of the unit cells are adjusted by means of an eight-dimensional Boltzmann-annealed amoeboid simplex (a mathematical creature which crawls around parameter space searching for an optimum answer) until the porosity

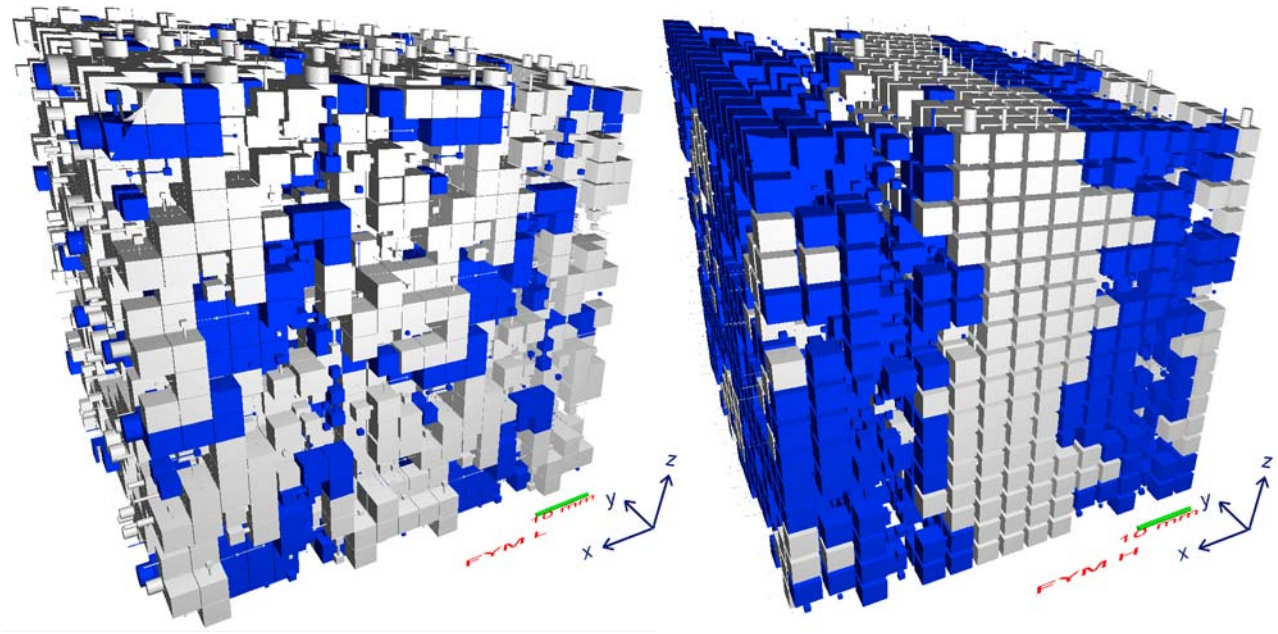

Figure 1. Simulations of the structures of 6 cm cubes of the FYM soil under (left) low compaction and (right) high compaction, with water (blue) drained to a tension of 29.1 kPa displaced by air (blue) corresponding to drainage of accessible throats of diameter 10 μm.

and percolation characteristics of the simulated network closely match the experimental data.

[11] For the sake of computational simplicity, the previous void structure model incorporated a log/linear throat size distribution; that is, a linear variation in the number of throats when plotted against a logarithmic size axis. Such a distribution dropped abruptly to zero, in boxcar fashion, at the maximum and minimum throat sizes corresponding to the experimental tensions, and was thus counterintuitive. The new log/Euler beta throat size distribution within the Pore-Cor void network encompasses more realistic and more flexible Gaussian-like, Poisson-like and bimodal distributions. The probability density function, representing the probability that the distribution lies in a small interval $[x, x + dx]$ is

$$f(x:\zeta,\eta) = \frac{1}{\Psi(\zeta,\eta)} x^{\zeta-1}(1-x)^{\eta-1} \tag{3}$$

where

$$\Psi(\zeta,\eta) = \int_0^1 x^{\zeta-1}(1-x)^{\eta-1} dx \tag{4}$$

is the Euler beta function.

[12] The parameters ζ and η are related to the mean μ and standard deviation σ of the distribution as follows:

$$\mu = \frac{\zeta}{\zeta+\eta} \tag{5}$$

$$\sigma^2 = \frac{\zeta\eta}{(\zeta+\eta)^2(\zeta+\eta+1)} \tag{6}$$

[13] These expressions may be recovered by using the result that:

$$\Psi(\zeta,\eta) = \frac{\Gamma(\zeta)\Gamma(\eta)}{\Gamma(\zeta+\eta)} \tag{7}$$

where the Euler gamma function is defined as:

$$\Gamma(x) = \int_0^\infty t^{x-1} e^{-t}\, \mathrm{d}\, t \tag{8}$$

and noting that:

$$\Gamma(x) = (x-1)\Gamma(x-1). \tag{9}$$

[14] The expressions for the mean and standard deviation may be inverted:

$$\zeta = \frac{\mu^2 - \mu^3 - \mu\sigma^2}{\sigma^2}, \tag{10}$$

$$\eta = \frac{\mu - 2\mu^2 + \mu^3 - \sigma^2 + \mu\sigma^2}{\sigma^2}. \tag{11}$$

The distribution is therefore completely specified if μ and σ, and therefore the quantities on the right hand side, are known.

[15] A network fitting parameter called "throat spread" is defined as twice the standard deviation σ. It is scaled so that values around 0.55 give linear distributions of relative number plotted against the logarithm of size or tension, lower values give Gaussian- or Poisson-like distributions, and greater values give bimodal distributions. The parameter

"throat skew" has a more complex definition in order to allow a balanced sampling of the simplex parameter space. It requires four quantities. The first two are the minimum $\mu_{\min}$ and maximum $\mu_{\max}$ possible means for a given standard deviation.

$$\mu_{\min} = \frac{1}{2}\left(1 - \sqrt{1 - 4\sigma^2}\right) \tag{12}$$

$$\mu_{\max} = \frac{1}{2}\left(1 + \sqrt{1 - 4\sigma^2}\right) \tag{13}$$

These can be found by substituting the following conditions into (8) and (9):

$$\zeta = \eta = 0. \tag{14}$$

[16] If there exists a region where the distribution is unimodal for a given standard deviation then we define the minimum and maximum unimodal means as μ_1 and μ_2 respectively. The boundary case is a uniform distribution with $\zeta = \eta = 1$. Values of μ_1 and μ_2 are obtained by solving a cubic equation, and then choosing the correct root (i.e., the one nearest the median, which is always 0.5) [*Press et al.*, 1986]:

$$\mu^3 - \mu^2 + \mu\sigma^2 + \sigma^2 = 0. \tag{15}$$

By default, a pore's size (length of each side of the cube) is equal to the size (diameter) of the largest throat that intersects it. Let the cumulative throat size distribution function be $F(\zeta, \eta, x)$. This is the probability that a throat will be smaller than x. If the throat positions are uncorrelated, the probability that all the n intersecting throats will be smaller than x is $F(\zeta, \eta, x)^n$. Another way of viewing this is as the cumulative size distribution of the largest intersecting throat. The probability density function for the pore sizes is therefore:

$$\begin{aligned}\frac{\mathrm{d}}{\mathrm{d}x}F(\zeta,\eta,x)^n &= nF(\zeta,\eta,x)^{n-1}f(\zeta,\eta,x)\\ &= \frac{n}{\Psi(\zeta,\eta)^n}\left\{\int_0^x t^{\zeta-1}(1-t)^{n-1}\mathrm{d}t\right\}^{n-1} x^{\zeta-1}(1-x)^{\eta-1}\end{aligned} \tag{16}$$

where the function f is the derivative of the function F. In practice, this distribution usually generates structures with too low a porosity, owing to inefficient packing together of the void features. The pore sizes are therefore bulked up by multiplying all their sizes by a parameter called "pore skew." The distribution is then truncated at the original maximum size to prevent the pores overlapping, and all pores larger than this size allocated the maximum size.

[17] Three of the dimensions of the parameter space explored by the simplex as its fits the model to experimental data are related to μ and σ (equations (3) to (15)) and the pore skew (equation (16)). Others are the network connectivity and short-range size autocorrelation function [*Matthews et al.*, 1995]. There are also three Boolean simplex parameters, namely whether the network can be generated without geometrically overlapping features, whether it can be adjusted to achieve the experimental porosity, and whether the network is fully interconnected.

2.2. Saturated Hydraulic Conductivity of the Network

[18] The network simulator can also calculate the permeability and saturated hydraulic conductivity of the simulated porous structures. It is assumed that Poiseuillian flow occurs across the whole unit cell in the $-z$ direction:

$$\left(\frac{\mathrm{d}V}{\mathrm{d}t}\right)_{\mathrm{cell}} = -\frac{\pi}{8\nu}\underset{cell}{\Omega}\left(F_{\mathrm{arcs}}\right)\frac{\delta P_{\mathrm{cell}}}{l_{\mathrm{cell}}} \tag{17}$$

where $\mathrm{d}V/\mathrm{d}t$ is the volume flow rate, ν is the fluid viscosity, and $\delta P_{\mathrm{cell}}/l_{\mathrm{cell}}$ is the pressure gradient across a single unit cell. $\underset{cell}{\Omega}$ is an averaging operator over the whole unit cell, operating on the flow capacities of the pore-throat-pore arcs (F_{arcs}) [*Matthews et al.*, 1993], and calculated by means of the Dinic network analysis algorithm [*Ahuja et al.*, 1997].

[19] A combination of equation (17) with the Darcy equation results in this expression for the Darcy permeability k of the unit cell, to which the hydraulic conductivity is directly related:

$$k = \frac{\pi}{8}\underset{cell}{\Omega}\left(F_{\mathrm{arcs}}\right)\frac{l_{\mathrm{cell}}}{A_{\mathrm{cell}}} \tag{18}$$

2.3. Saturated Hydraulic Conductivity From Water Retention

[20] We compare the results of the approach just described with a simpler statistical approach to derive saturated hydraulic conductivity from water retention data [*Campbell*, 1985; *Childs and Collis-George*, 1950]. A model is formed by considering the interconnection of cylinders of different sizes across a section of a porous material. We consider a special case in which it is assumed that these interconnections are random.

[21] A distribution $F(r)$ of cylindrical pore radii r is derived from the water retention curve (θ, h) as

$$F(r) = \frac{\mathrm{d}\theta}{\mathrm{d}r} = \frac{\mathrm{d}\theta}{\mathrm{d}h}\frac{\mathrm{d}h}{\mathrm{d}r} \tag{19}$$

where h is the tension. Assuming that the flow of water through a cylinder is proportional to its cross-sectional area, then

$$k \propto \left[\int_0^{r_{\max}} rF(r)\mathrm{d}r\right]^2 \tag{20}$$

[22] Usually this expression is incorporated into a model for relative permeability or unsaturated hydraulic conductivity, appearing as a denominator in such a model [*Mualem*, 1976]. A constant of proportionality is required to achieve absolute values of k from equation (20). Equation (20) may be rewritten as

$$k \propto \left[\int_0^{\theta_{sat}} \frac{1}{h}\mathrm{d}\theta\right]^2 \tag{21}$$

[23] Following *van Genuchten* [1980], we use the van Genuchten function for water retention to evaluate this integral, using the standard constraint $m = 1 - 1/n$ for the water retention parameters.

Table 1. Basic Properties of the Three Soils[a]

Soil	FYM	PKMg	NW
Location	Harpenden, Herts	Harpenden, Herts	North Wyke, Devon
Field	Broadbalk	Broadbalk	Rowden
GB national grid reference	TL121134	TL121134	SX652994
Latitude	51:48:36	51:48:36	50:46:43
Longitude	00:22:30	00:22:30	03:54:50
Soil type, SSEW group[b]	Paleoargillic brown earth	Paleoargillic brown earth	Stagnogley soil
Soil type, SSEW series[c]	Batcombe	Batcombe	Hallsworth
Soil type, FAO[b]	Chromic Luvisol	Chromic Luvisol	Gleyic Luvisol
Land use	arable, farmyard manure	arable, fertilized	permanent grass
Sand, 2000–63 μm (g g^{-1} dry soil)	0.222	0.183	0.147
Silt, 63–2 μm (g g^{-1} dry soil)	0.545	0.571	0.396
Clay, <2 μm (g g^{-1} dry soil)	0.233	0.246	0.457
Texture, SSEW classification[b]	clay loam	silty clay loam	clay
Particle density (g cm^{-3})	2.508	2.560	2.466
Organic matter (g g^{-1} dry soil)	0.048	0.015	0.076

[a]Abbreviations are as follows: FAO, U.N. Food and Agriculture Organization World Reference Base for Soil Resources classification system (approximation); FYM, farmyard manure; GB, Great Britain; PKMg, fertilized inorganically; NW, North Wyke; SSEW, Soil Survey of England and Wales classification system. Latitude is given in deg:min:sec N, and longitude is given in deg:min:sec W.
[b]From *Avery* [1980].
[c]From *Clayden and Hollis* [1984].

With the change of variable

$$\Theta = \frac{\theta - \theta_r}{\theta_s - \theta_r} \tag{22}$$

Equation (21) becomes

$$k \propto (\theta_s - \theta_r)^2 \left[\int_0^{1_{sat}} \frac{1}{h} \mathrm{d}\Theta \right]^2 \tag{23}$$

which we may rewrite as

$$k \propto \alpha^2 (\theta_s - \theta_r)^2 \left[\int_0^{1_{sat}} \left(\frac{\Theta^{1/m}}{1 - \Theta^{1/m}} \right)^{1-m} \mathrm{d}\Theta \right]^2 \tag{24}$$

where α is the third fitting parameter for the van Genuchten function. The integral in equation (24) equates to 1 and k becomes

$$k \propto \alpha^2 (\theta_s - \theta_r)^2. \tag{25}$$

A constant of proportionality needed to achieve absolute values may be inserted in equation (25) to yield:

$$k = \frac{\rho g}{8\nu} \left(\frac{2\gamma}{\rho g} \right)^2 \alpha^2 (\theta_s - \theta_r)^2 \tag{26}$$

where ρ is the density of water, g is the acceleration due to gravity, and γ is the surface tension of water. Here we assume no requirement for a correction factor to account for tortuosity. Equation (26) simplifies to

$$k = \frac{\gamma^2}{2\nu\rho g} \alpha^2 (\theta_s - \theta_r)^2. \tag{27}$$

3. Experimental Methodology

3.1. Soils

[24] Soils were chosen from the Broadbalk Winter Wheat classical experiment at Rothamsted Research in Hertfordshire and from the Rowden experiment at North Wyke (NW) Research in Devon as being representative of typical arable and grassland agricultural land management in the United Kingdom, respectively. Samples were taken from the upper 150 mm of the organic farm yard manure (strip 2.2) and inorganic PKMg (strip 5) treatments at Broadbalk, and from the same depth in an undrained and unfertilized treatment at Rowden. The three soils are termed FYM, PKMg and NW. Each soil was crumbled to pass a 4 mm sieve and left to air dry in a single bulked sample. The soils were then equilibrated at 0.16 g g^{-1} water content by adding deionized water, and stored in air-tight containers at 4°C until ready. Deionized water was used as standard for all experiments, in the knowledge that our soils either had low active-clay contents (PKMg and FYM) or were sufficiently stabilized by organic matter (NW) that destructuring by any osmotic swelling was negligible.

3.2. Basic Soil Properties

[25] Basic soil properties were measured by standard methods (Table 1). Organic matter was removed with H_2O_2, and the particles dispersed with $[NaPO_3]_6$. Soil particle size distribution was then determined by a combination of wet sieving of 60 μm to 2 mm particles (British Standard 1377, 1975) and X-ray attenuation during sedimentation of particles smaller than 60 μm in a SediGraph 5100 (Micromeritics Instrument Corporation, Norcross, GA, USA). Particle density was measured by the pycnometer method [*Blake and Hartge*, 1986], in which deionized water is displaced by oven-dried soil. Soil organic matter was calculated by the loss-on-ignition method.

3.3. Soil Water Release Characteristic

[26] As there was no single apparatus that would equilibrate the soils at the range of matric potentials of interest (from 0 to −1500 kPa), two sets of samples were prepared: one set for "dry-end" potentials in the range −13 to −1500 kPa, and one for "wet-end" potentials in the range 0 to −10 kPa.

[27] Soil that was to be equilibrated at dry-end matric potentials was taken from the single equilibrated sample

and packed to fill small stainless steel cores (i.d., 54 mm; h, 25 mm) at compacting pressures of either 174 or 522 kPa to create two structures using a pneumatic soil press. These compaction pressures are hereafter termed L (low) and H (high). Twenty-four replicate cores for each of the six soil compaction treatments were created in this manner. All cores were brought to saturation by standing in free water and then two or three replicate cores were equilibrated at either −13, −20, −30, −50, −100, −200, −300, −500, −1000 or −1500 kPa matric potential for 28 days in a pressure chamber apparatus. At equilibration, the soil height and diameter were measured with digital calipers before oven-drying at 105°C for 48 h.

[28] Soil that was to be equilibrated at wet-end matric potentials was packed at the same two compacting pressures to fill the same size cores to within 3 mm of the top. The exact height of the soil in the cores was determined using the digital calipers and the core was weighed at this point. The remainder of the core volume was filled with a wet 1:1 (w:v) suspension of Plaster of Paris ($CaSO_4 \cdot 0.5H_2O$). A spatula was used to ensure good contact with the soil below and a flat surface on the top. The plaster set very quickly and the cores were reweighed. Four replicate cores were prepared for each soil compaction treatment. Each replicate core, with the plaster facing down, was placed on one of four ceramic tension plates connected to a hydraulic column and brought to saturation by standing in free water. The soil mass at saturation (0 kPa matric potential) was recorded, and the height and diameter were measured using digital calipers. The water level in the hydraulic column was then lowered to 5.1 cm below the level of the tension plate to give a matric potential of −0.5 kPa. The mass was recorded daily until it did not differ significantly from the previous day ($P > 0.05$ by Student's t test). At this point the height and diameter were recorded and the water level in the hydraulic column was lowered a further 5.1 cm to create a matric potential of −1 kPa. The process of equilibrating, weighing and measuring was continued through decrements of 0.5 kPa to a matric potential of −10 kPa. As with the ceramic of the tension plates, it was assumed that the plaster layer remained saturated in this range of matric potentials such that a hydraulic connection was maintained between the soil and the water level. At the end the soil was oven-dried at 105°C for 48 h.

[29] Through knowing the mass, height and diameter of the soil, the soil water characteristic could be expressed in gravimetric terms, and the volume change at different matric potentials could be estimated.

3.4. Soil Conductivity Characteristic

[30] The effect of compaction on hydraulic conductivity was measured using a triaxial cell apparatus. Two replicate cores (d, 50 mm; h, 100 mm) of each of the equilibrated soils were made to an initial compacting pressure of 100 kPa using a pneumatic press and a brass corer with a longitudinal split. The soil core was removed from the corer, placed inside a rubber membrane and placed in a GDS STDTTS triaxial system (GDS Instruments Ltd, Hook, Hants, United Kingdom) which was filled with water. The soil was brought steadily to saturation through increasing the cell (radial) pressure and the pore water pressure in tandem up to 1000 kPa to force water into the pores while restricting volume change. The quantity of water entering the soil was monitored, having an estimation of the initial water-filled pore volume, and a pore pressure coefficient test was carried out which returned a value close to 1. Both of these confirmed that saturation was successful.

[31] Following saturation, the soil was consolidated by increasing the cell pressure above that of the pore water pressure to give an effective stress. Progressive effective stresses of up to 600 kPa were subjected on the soil, and at each stress, the saturated hydraulic conductivity was measured by passing water through the soil by way of two pressure volume controllers connected to the upper and lower surfaces of the soil.

3.5. Soil Consolidation Characteristic

[32] The saturated consolidation characteristic was measured to give further insight into the effect of consolidation on porosity. From the equilibrated sample, two replicate cores of the FYM and PKMg soils and one replicate of the NW soil were made as described above for the conductivity characteristic, except to a compacting pressure of 174 kPa. The core was placed inside a GDSTAS loading frame triaxial system (GDS Instruments Ltd, Hook, Hants, United Kingdom). The soil was saturated as described above and then subjected to progressive isotropic effective stresses of up to 900 kPa. Volume change was monitored by displacement in a water-filled inner cell system [*Ng et al.*, 2002] and was converted to porosity. Porosity expressed as a function of effective stress was modeled with an asymmetrical sigmoidal Gompertz function, allowing the preconsolidation stress and consolidation index to be calculated [*Gregory et al.*, 2006]. The preconsolidation stress describes a threshold stress in the consolidation characteristic between elastic or recoverable volume change, and plastic or irreversible volume change, reflecting the stress history of the soil. The consolidation index is the slope of the consolidation characteristic (volume loss) as a linear function of the logarithm of consolidation stress in its plastic normal consolidation phase beyond the preconsolidation stress. The greater the value, the more susceptible the soil is to porosity loss when subjected to stress. As the effective consolidation stress was common to the measurements of both conductivity and consolidation characteristics, the relationship between porosity and conductivity could be examined.

4. Experimental Results

4.1. Soil Water Release Characteristic

[33] Soil water release characteristics of the three soils are shown in Figure 2 at the two compaction pressures. Water retention was greater for the NW soil than the PKMg and FYM soils ($P < 0.05$). Of the two arable soils, more water was retained by the FYM treatment than the inorganically fertilized (PKMg) treatment ($P < 0.05$). Compaction had a clear effect on water retention at matric potentials in the range 0 to −10 kPa ($P < 0.05$), but little effect on the dry end.

[34] Using soil particle density values (Table 1) and neglecting residual water retention at −1500 kPa, the water characteristics of the soils were converted into graphs of the accessible void volume occupied by air against the intruded feature size (Figure 3). Intruded feature sizes

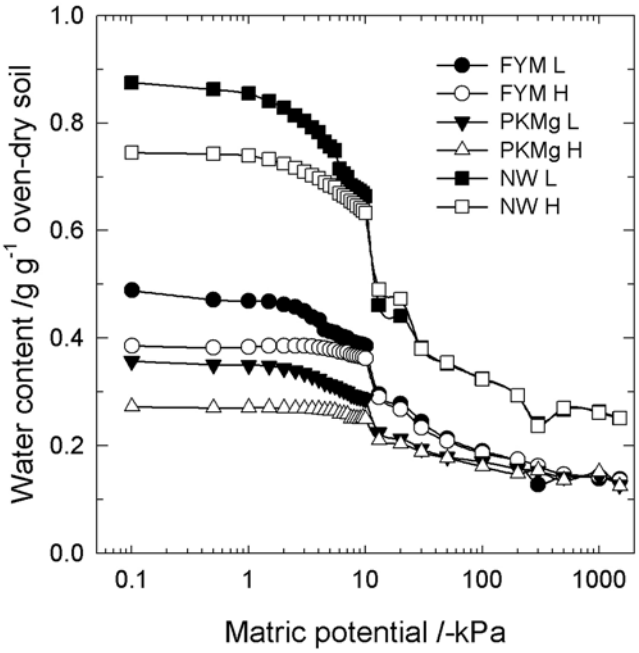

Figure 2. The soil water release characteristic of the farmyard manure (FYM), fertilized inorganically (PKMg), and North Wyke (NW) soils compacted at 174 kPa (low (L)) and 522 kPa (high (H)).

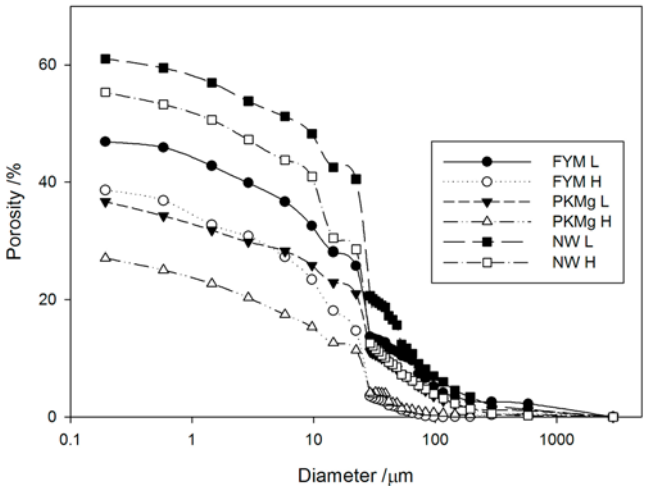

Figure 3. Conversion of the soil water release characteristic measurements from the accurate gravimetric/tension characteristic of Figure 2 to a more approximate volumetric/void diameter characteristic for modeling purposes.

were calculated from the Laplace equation (28), which gives the diameter d of a cylinder which can be intruded by a nonwetting fluid (air displacing water) at an applied differential pressure h:

$$d = \frac{4\gamma \cos\theta}{h}. \quad (28)$$

[35] It was assumed that the interfacial tension γ of water in soil is 0.075 N m^{-1} and that water is fully wetting so that $\theta = 0°$, although in practice it becomes less wetting with higher organic carbon content [*Matthews et al.*, 2008].

[36] The data shown in Figure 3 were used for the network modeling of the void space. The porosity values for the soil sample, in volume percentage, are shown in Table 2, assuming that the soil does not change volume during the water release. This prevalent approximation is necessary for the model, which comprises a network of a single porosity for each sample that replicates the entire water release characteristic. Volume changes were estimated during the soil water release characteristic, and were found to be negligible for matric potentials between 0 and −10 kPa, but that all soils lost pore volume through shrinkage at lower (more negative) potentials, particularly the NW soil owing to its greater clay content.

4.2. Soil Conductivity Characteristic

[37] The effect of stress on saturated hydraulic conductivity can be seen in Figure 4. The NW soil has the highest conductivity at low stress, and has a greater response to stress. The graph shows the 174 and 522 kPa stresses that correspond to the L and H compaction treatments prior to measurements of the soil water release characteristic (see Figure 2). The relationship between saturated hydraulic conductivity and effective stress followed a power law model, and so linear regression was performed on logarithmically transformed data. It can be seen that the prediction of conductivity at 522 kPa involved extrapolation for the NW soil above the highest measurable conductivity data at a stress of 300 kPa.

4.3. Soil Consolidation Characteristic

[38] The soil consolidation characteristic traces the reduction in porosity with increasing stress (see Figure 5). Initial porosities were much greater for the NW soil than the FYM soil, which in turn was greater than for PKMg soil. The porosity of the NW soil at 1000 kPa was still greater than that of the arable soils at low stresses.

[39] The consolidation indices are given in Table 3 and reflect the inherent differences between the soils. Although the preconsolidation stress is to some extent artificial in this piece of work, being based on repacked cores, it can be seen that the NW soil withstood a greater consolidation stress prior to normal consolidation. Once the preconsolidation stress is exceeded, the soil undergoes normal consolidation. The consolidation index was greatest for the NW soil followed by the FYM soil, showing that the NW soil was least

Table 2. Saturated Hydraulic Conductivity of the Soils as Given by the Regressions Shown in Figure 4[a]

Soil	Effective Stress[b] (kPa)	Effective Porosities of the Soils as Used by the Network Model	Saturated Hydraulic Conductivity (cm s^{-1})
FYM	174	0.469	1.91×10^{-7}
	522	0.386	3.31×10^{-8}
PKMg	174	0.366	1.38×10^{-8}
	522	0.271	2.88×10^{-9}
NW	174	0.610	3.87×10^{-8}
	522	0.553	6.25×10^{-10}

[a]Abbreviations are as follows: FYM, farmyard manure; NW, North Wyke; PKMg, fertilized inorganically.
[b]Effective stress of 174 kPa is low, and effective stress of 522 kPa is high.

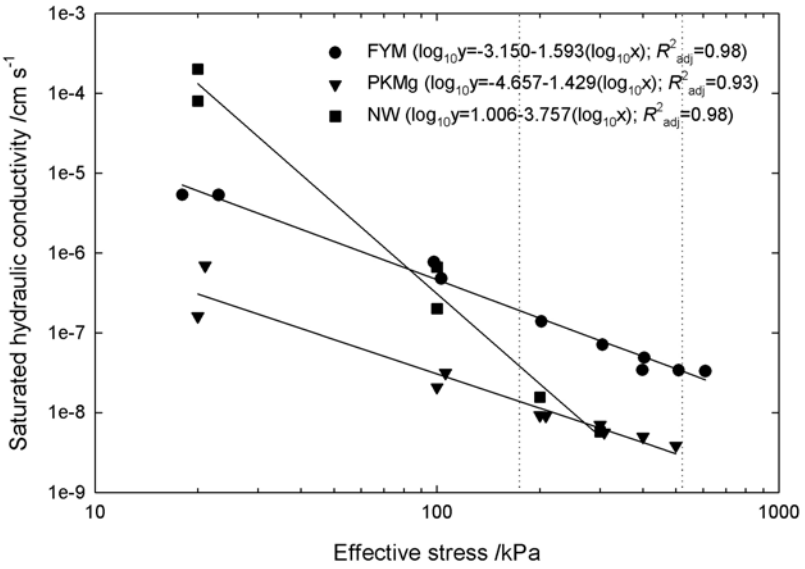

Figure 4. The effect of effective consolidation stress on the saturated hydraulic conductivity of the three soils. The symbols give the measured conductivity, and the lines give the function on logarithm-transformed data. Dotted lines are shown at 174 and 522 kPa.

resistant to volume change once the preconsolidation stress was exceeded.

[40] Figure 6 shows the porosity-conductivity characteristic derived for the three soils. It highlights the greater porosity of the NW soil, and the sharp decreases in conductivity as porosity is reduced by consolidation.

[41] It should be noted that the consolidation stresses of the conductivity experiment (Figure 4) for the FYM and PKMg soils were considerably greater than those associated with the consolidation characteristic (Figure 5). Therefore extrapolation of the consolidation characteristic was necessary to estimate the porosity of these two soils at consolidation stresses greater than 200 kPa.

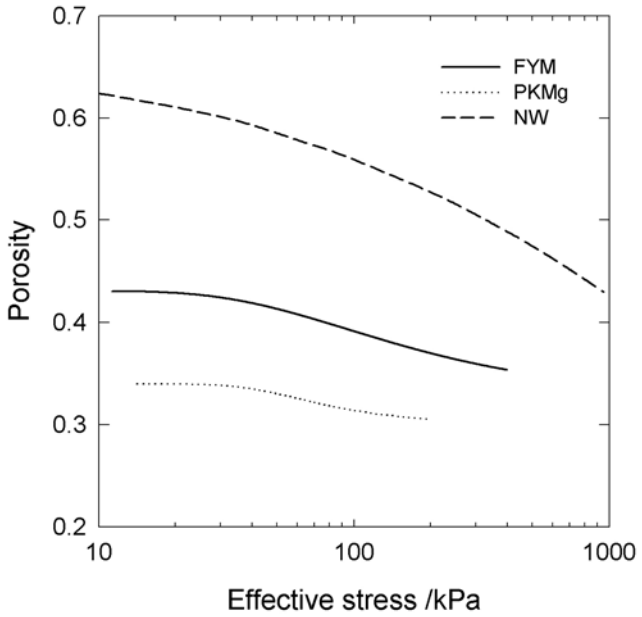

Figure 5. The consolidation characteristic of the three soils.

4.4. Modeling Results

[42] The modeling of the porous network was carried out by using the simplex to find modeling parameters which generated network structures which matched the porosity relatively to within 0.1% of the experimental value and that had water retention characteristics that also closely matched the experimental results. Ten different stochastic realizations were generated for each soil type and treatment. For the simulation of hydraulic conductivity, the conductivities of all ten structures were calculated and averaged for each sample. However, since the modeling parameters are coupled into concerted convergences onto the experimental data, the averages of single parameters are not meaningful. Therefore, to find a representative modeled structure for each sample, the stochastic realizations with any of the fitting parameters showing a deviation from the mean larger than the standard deviation were discarded. Out of the remaining stochastic realizations, the realization showing the smallest value of distance between experimental and simulated water characteristic was chosen as representative.

[43] The modeling parameters for each of the representative structures are shown in Table 4. The percentage distances between simulated and experimental curves shown in the right hand column were calculated by plotting the curves

Table 3. Consolidation Indices of the Three Soils Derived From Modeling the Consolidation Characteristic in Figure 5

	Goodness of Fit of Model				
Soil	P	R^2_{adj}	Inflection (kPa)	Preconsolidation Stress (kPa)	Consolidation Index
FYM	<0.001	0.944	95	32	0.077
PKMg	<0.001	0.673	60	35	0.059
NW	<0.001	0.995	698	67	0.145

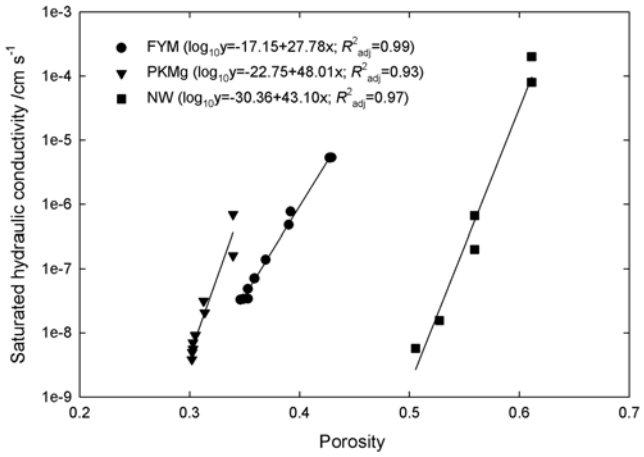

Figure 6. The porosity-conductivity characteristic derived for the three soils on the basis of the data shown in Figures 4 and 5 and lognormal fitting functions.

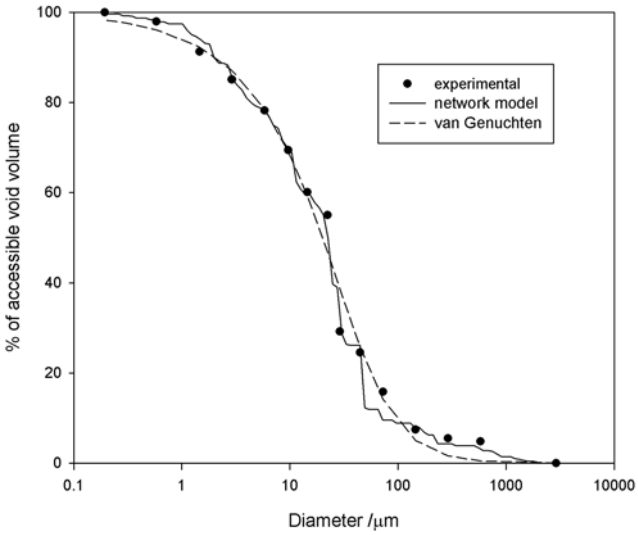

Figure 7. Comparison of network model fit and van Genuchten fit for farmyard manure (low) water retention data. The radii of the experimental points have been scaled to 1% of the range of the experimental data on each axis.

on a graph with logarithmic horizontal axis (size or tension), and a linear vertical axis, with the spread of the experimental points being 100% in each direction. The distances between each experimental point and all the simulated points were calculated. The closest distances between experiment and simulation were then averaged over the number of experimental points to give the distances shown in Table 4. A typical fit (1.2% for FYM L) is shown in Figure 7, in which the size of each of the experimental points is scaled such that if the simulation just touches it, it has matched to 1% of the spread on each axis. It can be seen in Table 4 that the distances between the simulated and the experimental water retention curves are always below 1.4% and in one case below 1%. This compares favorably with fits using the previous log linear throat size distribution applied to soil structure under grass and clover, where the average distances were 2.4% and 1.9% for fits to only 7 experimental measurements per water retention curve [*Holtham et al.*, 2007].

4.5. Pore and Throat Size Distribution

[44] All the modeled structures of the soils at the low compaction level (L) show a bimodal throat size distribution, as indicated by the values of throat spread in Table 4 which are all larger than 0.55. These bimodal distributions give the sigmoidal cumulative distributions, shown as solid triangles in Figures 8–10. Simulated structures of the soils at the high compaction level (H) show a unimodal throat size distribution in the FYM soil, bimodal throat size distribution in the NW soil and a very slight bimodal distribution in the PKMg soil (see Table 4 and solid circles in Figures 8–10). It can be seen that for all the soils there are fewer larger throats for the soil compacted at higher pressure. In the case of the NW soil (Figure 10) the difference between the throat size distributions of the two soil compaction levels is much smaller than in the FYM and PKMg soils. This may in part be due to the water content of the soils when they were initially made at the L and H compaction states. As the NW soil has a greater clay content, more water is required to achieve plasticity than in the lighter-textured FYM and PKMg soils.

[45] However, the simulated pores in the model increase in size on compaction; that is, the H pore size distributions (open circles) are at higher size ranges than the L distributions (open triangles), with truncation above 2910 μm (to prevent them overlapping) as shown. This behavior is also very evident in Figure 1, in which the increased pore sizes of the compacted structure mask the change in throat sizes. Such behavior is clearly incorrect in the light of the obvious interpretation of the water retention curves in Figure 2, and also in the context of the findings of other workers described in section 1.2. It is discussed below.

Table 4. Network Modeling Parameters of the Representative Structures and Percentage Distances Between Simulated and Experimental Water Retention Curves[a]

Soil	Connectivity	Throat Skew	Throat Spread	Pore Skew	Correlation Level	Distance (%)
FYM high	3.162	−25.73	0.482	557.1	0.540	0.98
FYM low	3.128	−25.94	0.792	2.59	0.121	1.21
PKMg high	3.158	−31.51	0.566	590.2	0.402	0.83
PKMg low	4.290	−42.95	0.579	13.8	0.369	1.02
NW high	3.230	−26.64	0.653	19.7	0.201	1.41
NW low	3.142	−25.26	0.650	16.5	4.00E-02	1.16

[a]The minimum and maximum modeled throat diameters and pore sizes were 0.194 μm and 2.910 mm, respectively, for all the samples. Abbreviations are as follows: FYM, farmyard manure; NW, North Wyke; PKMg, fertilized inorganically.

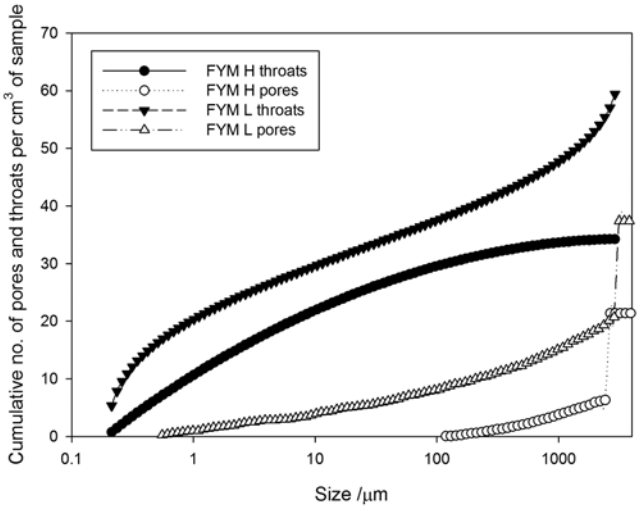

Figure 8. Cumulative pore and throat size distribution of the simulated farmyard manure (FYM) soil samples.

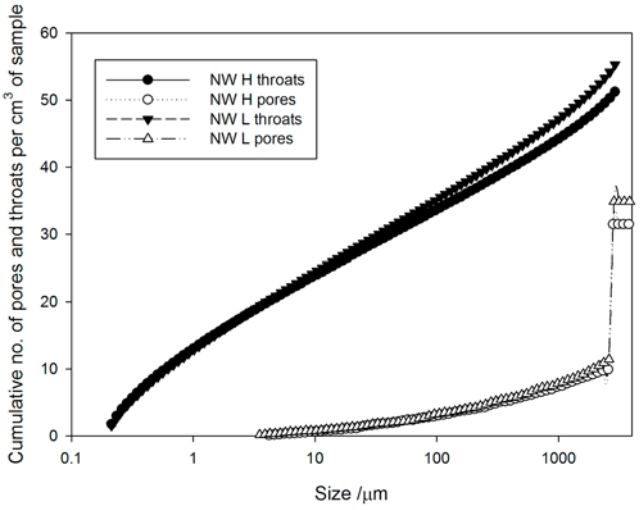

Figure 10. Cumulative pore and throat size distribution of the simulated North Wyke (NW) soil samples.

4.6. Hydraulic Conductivity

[46] The mean values of simulated hydraulic conductivity for FYM and PKMg soils show the expected trends (Figure 11) with lower hydraulic conductivity for structure compacted at higher pressures. For the NW soil there is little difference after compaction. The means of these values were compared with an unpaired independent two-tail Student's *t* test to ascertain whether the differences in the mean values for low and high compaction for each soil are statistically significant. This test is merely showing whether the stochastic nature of the modeling masks the variation in hydraulic conductivity due to compaction, and has no bearing on the experimental measurements. The *t* test *P* statistic was 0.33, 0.12 and 0.49 for the FYM, PKMg and NW soils, respectively, showing relatively high probabilities that the null hypothesis, that the means are identical, is correct. The simulated saturated hydraulic conductivities must therefore be viewed with caution, in the knowledge that the stochastic variations in the model are high with respect to the effects of compaction. In the case of the NW soil, the water retention curves, and hence H and L modeled structures, are very similar in terms of simulated pore and throat size distribution, so the high P statistic of 0.49 is not surprising.

[47] The van Genuchten model was fitted to the six water retention data sets, yielding the parameters shown in Table 5. An example fit for FYM L is shown in Figure 7, with a closeness of 1.8% compared to 1.2% for the network model.

[48] Using the simpler approach derived from that of *Childs and Collis-George* [1950], equation (27), we obtained the values for K_s shown in Figure 11. It can be seen that overall the modeled hydraulic conductivities are closer to experimental values than those derived from the simpler approach. However, all the values overestimate the experimental measurements, and the network simulated values and those from the simpler approach tend to vary in a concerted fashion.

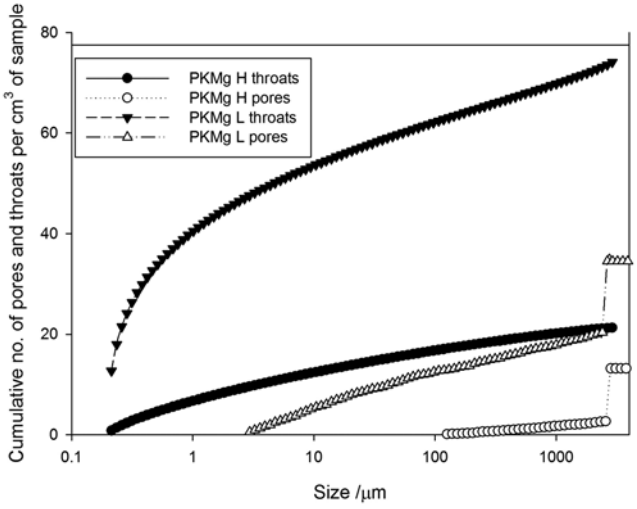

Figure 9. Cumulative pore and throat size distribution of the simulated fertilized inorganically (PKMg) soil samples.

5. Discussion

5.1. Experimental Discussion

[49] When drawing conclusions, it must be remembered that exact water retention curves are impossible to measure, because the soil samples need to be saturated at the start, and this can cause swelling of the unconfined soil. This was a particular problem with the NW soil at high compaction. Nevertheless the experimental results show a clear difference between the three soils. The NW soil was clayey in texture and had a greater organic matter content deriving from its permanent grassland land use. It thus had an inherently better-developed structure with greater porosity and stability. This was reflected in both the water release and consolidation experiments, as the NW soil retained more water at each matric potential and had a greater porosity at all effective stresses. At an effective stress of 1000 kPa, the NW soil had a greater porosity than the PKMg and FYM soils did at 10 kPa. For the two arable soils, the FYM soil, which receives an organic amendment as part of its management, had a greater porosity and greater water retention than the inorganically fertilized PKMg soil.

[50] Compaction in the water release experiment and consolidation in the triaxial experiments had adverse effects

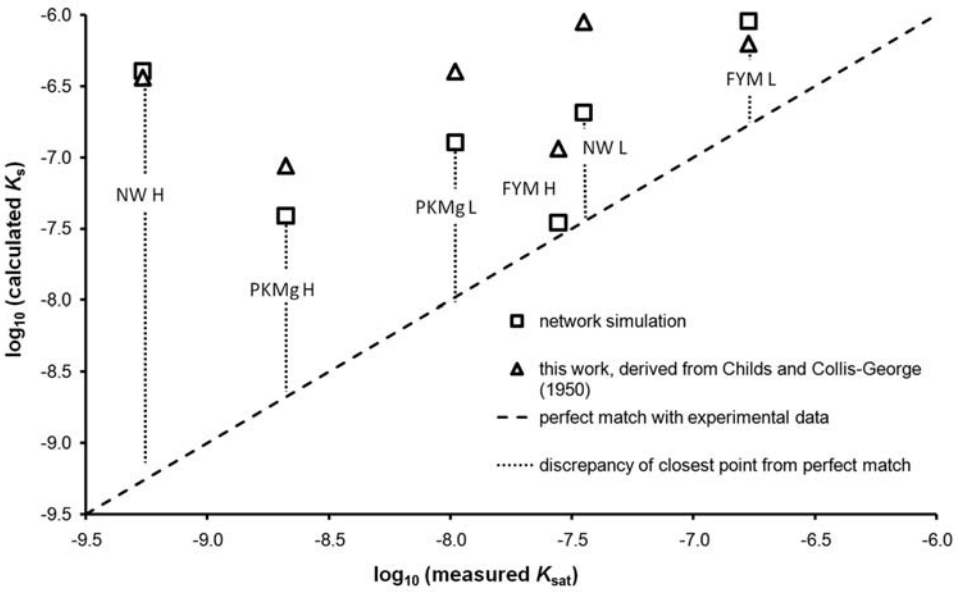

Figure 11. Comparison of network and van Genuchten/Mualem saturated hydraulic conductivity values with experimental values.

on all soils. The compaction treatment had a clear effect on water retention at matric potentials greater than −10 kPa. This corresponds to pores greater than 30 μm equivalent cylindrical diameter. Pores smaller than 30 μm appeared to be unaffected as the water release characteristics were the same for the L and H compaction treatments in each soil. In general, the stability of a soil pore is inversely related to its size and hence compacting a soil to 522 kPa would result in a greater loss of larger pores than compaction to 174 kPa. As a matric potential of −10 kPa might be considered to represent "field capacity," then our findings suggest that the greater structural damage done at 522 kPa compared to 174 kPa might be manifest in a reduced ability to permit water transmission following saturation by gravitational drainage, rather than affecting the plant-available water supply in the soil.

[51] Combining the two consolidation experiments to give the porosity/saturated hydraulic conductivity relationship shows the dramatic changes in hydraulic conductivity resulting from small changes in porosity. These results confirm the importance of factors other than porosity in mediating flow; a scaling of the whole pore space to match the reduction in porosity could not possibly account for the observed changes in hydraulic conductivity. Typically models linking porosity to hydraulic conductivity also include reference to critical pore scales, *Carman* [1939]. The equation derived in this paper from the Collis-George model falls into this class. Equally the use of the Pore-Cor void network simulator explicitly and mechanistically accounts for the role of pore throats in controlling hydraulic conductivity.

5.2. Modeling Discussion

[52] The Pore-Cor network simulation software models correctly the trend of throat size distributions for the arable soils. However, the model fails to describe fully the effect of compaction. The representative structures demonstrate a change of throat size distribution on compaction from bimodal to unimodel, and from larger to smaller sizes, which seems reasonable in the light of the water retention curves in Figure 2. Despite a statistically wide variation in the predicted saturated hydraulic conductivities, owing to the stochastic variability of the model, the representative structures show the correct trends, because the saturated hydraulic conductivity is dominated by the narrowed throats rather than the larger pores. However, the network model is unable to pack these smaller features sufficiently close together to achieve the correct porosity, and therefore can only obtain the experimental porosity by bulking up the pores using the pore skew parameter.

[53] As the experimental saturated hydraulic conductivity of the NW soil at high compression is based on an extrapolation, comparisons between this datum and the modeled results are less safe than the other comparisons.

[54] The approach followed in this paper may be regarded as complementary to recent research aimed at developing a mechanistic understanding of soil pore strain [*Berli et al.*, 2008]. These models seek to predict the detailed response of structure to compaction and the consequent effects on hydraulic function. While these models are at present restricted to simple idealized configurations of packed aggregates they hold potential to be upscaled to describe larger systems and associated pore networks. Clearly a means of inferring the structural response of such a network to compaction from experimental water release data, as

Table 5. The van Genuchten Fitting Parameters

	FYM Low	FYM High	PKMg Low	PKMg High	NW Low	NW High
θ_s	0.517	0.482	0.479	0.421	0.642	0.605
θ_r	0.139	0.187	0.1891	0.214	0.195	0.213
α	0.124	0.068	0.129	0.085	0.125	0.091

presented here, will be beneficial to the development, testing and validation of the predictive modeling of compaction.

6. Conclusions

[55] We have measured water retention, consolidation and saturated hydraulic conductivity characteristics of soil samples that illustrate the difference between different soil types (arable and grassland soils), and the effect of different treatments of an arable soil. These measurements are of interest in themselves, and a derived characteristic demonstrates a very high dependence of saturated hydraulic conductivity on porosity. The measurements are sufficiently closely spaced, in terms of tension or stress, to provide a severe test for the network model. The model shows reasonable and interesting changes on throat size distribution. It fits the water retention curves better than van Genuchten functions, and predicts changes in saturated hydraulic conductivity that are generally more accurate than those predicted by the simpler approach based on the work of Childs and Collis-George. However, the network model fails to represent the changes in pore size, owing to its inability to pack small features sufficiently close together. There is clearly a need for an explicitly dual porous network model of soil, which will now be the focus of our investigations.

[56] **Acknowledgments.** We are grateful for the advice of Deborah Holtham of North Wyke Research. Rothamsted Research and North Wyke Research are institutes of the UK Biotechnology and Biological Sciences Research Council (BBSRC). This work was supported by BBSRC grant BB/E001793/1.

References

Ahuja, R. K., M. Kodialam, A. K. Mishra, and J. B. Orlin (1997), Computational investigations of maximum flow algorithms, *Eur. J. Oper. Res.*, *97*, 509–542, doi:10.1016/S0377-2217(96)00269-X.

Alaoui, A., and B. Goetz (2008), Dye tracer and infiltration experiments to investigate macropore flow, *Geoderma*, *144*, 279–286, doi:10.1016/j.geoderma.2007.11.020.

Avery, B. W. (1980), *Soil Classification for England and Wales (Higher Categories)*, *Tech. Monogr. 14*, Soil Surv. of England and Wales, Harpenden, U. K.

Berli, M., A. Carminati, T. A. Ghezzehei, and D. Or (2008), Evolution of unsaturated hydraulic conductivity of aggregated soils due to compressive forces, *Water Resour. Res.*, *44*, W00C09, doi:10.1029/2007WR006501.

Blake, G. R., and K. H. Hartge (1986), Particle density, in *Methods of Soil Analysis: Part 1. Physical and Mineralogical Methods*, edited by A. Klute et al., pp. 377–382, Am. Soc. Agron., Madison, Wisc.

Boivin, P., B. Schaffer, E. Temgoua, M. Gratier, and G. Steinman (2006), Assessment of soil compaction using shrinkage modelling: Experimental data and perspectives, *Soil Tillage Res.*, *88*, 65–79, doi:10.1016/j.still.2005.04.008.

Borgesen, C. D., O. H. Jacobsen, S. Hansen, and M. G. Schaap (2006), Soil hydraulic properties near saturation, an improved conductivity model, *J. Hydrol.*, *324*, 40–50, doi:10.1016/j.jhydrol.2005.09.014.

Campbell, G. S. (1985), *Soil Physics With Basic Transport Models for Soil-Plant Systems*, Elsevier, New York.

Carman, P. C. (1939), Permeability of saturated sands, soils and clays, *J. Agric. Sci.*, *29*, 262–273, doi:10.1017/S0021859600051789.

Childs, E. C., and N. Collis-George (1950), The permeability of porous materials, *Proc. R. Soc. London, Ser. A*, *201*, 392–405.

Clayden, B., and J. M. Hollis (1984), *Criteria for Differentiating Soil Series*, *Tech. Monogr. 17*, Soil Surv. of England and Wales, Harpenden, U. K.

Coquet, Y., J. Simunek, C. Coutadeur, M. T. van Genuchten, V. Pot, and J. Roger-Estrade (2005), Water and solute transport in a cultivated silt loam soil: 2. Numerical analysis, *Vadose Zone J.*, *4*, 587–601, doi:10.2136/vzj2004.0153.

Davoudi, M. H., and G. Lefebvre (2005), Influence of compaction condition on the microstructure of a non-plastic glacial till, paper presented at the 16th International Conference on Soil Mechanics and Geotechnical Engineering, Int. Soc. Soil Mech. and Geotech. Eng., Osaka, Japan, 12–16 Sept.

Dexter, A. R., E. A. Czyz, G. Richard, and A. Reszkowska (2008), A user-friendly water retention function that takes account of the textural and structural pore spaces in soil, *Geoderma*, *143*, 243–253, doi:10.1016/j.geoderma.2007.11.010.

Gregory, A. S., W. R. Whalley, C. W. Watts, N. R. A. Bird, P. D. Hallett, and A. P. Whitmore (2006), Calculation of the compression index and precompression stress from soil compression test data, *Soil Tillage Res.*, *89*, 45–57, doi:10.1016/j.still.2005.06.012.

Holtham, D. A. L., G. P. Matthews, and D. S. Scholefield (2007), Measurement and simulation of the void structure and hydraulic changes caused by root-induced soil structuring under white clover compared to ryegrass, *Geoderma*, *142*, 142–151, doi:10.1016/j.geoderma.2007.08.018.

Johnson, A., I. M. Roy, G. P. Matthews, and D. Patel (2003), An improved simulation of void structure, water retention and hydraulic conductivity in soil, using the Pore-Cor three-dimensional network, *Eur. J. Soil Sci.*, *54*, 477–489, doi:10.1046/j.1365-2389.2003.00504.x.

Kawamoto, K., P. Moldrup, T. P. A. Ferre, M. Tuller, O. H. Jacobsen, and T. Komatsu (2006), Linking the Gardner and Campbell models for water retention and hydraulic conductivity in near-saturated soil, *Soil Sci.*, *171*, 573–584, doi:10.1097/01.ss.0000228035.72647.3c.

Kosugi, K. (1999), General model for unsaturated hydraulic conductivity for soils with lognormal pore-size distribution, *Soil Sci. Soc. Am. J.*, *63*, 270–277.

Matthews, G. P., A. K. Moss, M. C. Spearing, and F. Voland (1993), Network calculation of mercury intrusion and absolute permeability in sandstone and other porous media, *Powder Technol.*, *76*, 95–107, doi:10.1016/0032-5910(93)80045-C.

Matthews, G. P., A. K. Moss, and C. J. Ridgway (1995), The effects of correlated networks on mercury intrusion simulations and permeabilities of sandstone and other porous media, *Powder Technol.*, *83*, 61–77, doi:10.1016/0032-5910(94)02942-H.

Matthews, G. P., C. W. Watts, D. S. Powlson, J. C. Price and W. R. Whalley (2008), Wetting of agricultural soils measured by a simplified capillary rise technique, *Eur. J. Soil Sci.*, *59*, 817–823, doi:10.1111/j.1365-2389.2008.01039.x.

Mooney, S. J., and W. Nipattasuk (2003), Quantification of the effects of soil compaction on water flow using dye tracers and image analysis, *Soil Use Manage.*, *19*, 356–363, doi:10.1079/SUM2003210.

Mualem, Y. (1976), A new model for the predicting the hydraulic conductivity of unsaturated porous media, *Water Resour. Res.*, *12*, 513–522, doi:10.1029/WR012i003p00513.

Neuweiler, I., and O. A. Cirpka (2005), Homogenization of Richards equation in permeability fields with different connectivities, *Water Resour. Res.*, *41*, W02009, doi:10.1029/2004WR003329.

Ng, C. W. W., L. T. Zhan, and Y. J. Cui (2002), A new simple system for measuring volume changes in unsaturated soils, *Can. Geotech. J.*, *39*, 757–764, doi:10.1139/t02-015.

Oliver, Y. M., and K. R. J. Smettem (2005), Predicting water balance in a sandy soil: Model sensitivity to the variability of measured saturated and near saturated hydraulic properties, *Aust. J. Soil Res.*, *43*, 87–96, doi:10.1071/SR03146.

Or, D., and M. Tuller (1999), Liquid retention and interfacial area in variably saturated porous media: Upscaling from single-pore to sample-scale model, *Water Resour. Res.*, *35*, 3591–3605, doi:10.1029/1999WR900262.

Peat, D. M. W., G. P. Matthews, P. J. Worsfold, and S. C. Jarvis (2000), Simulation of water retention and hydraulic conductivity in soil using a three-dimensional network, *Eur. J. Soil Sci.*, *51*, 65–79, doi:10.1046/j.1365-2389.2000.00294.x.

Peng, X. H., R. Horn, B. Zhang, and Q. G. Zhao (2004), Mechanisms of soil vulnerability to compaction of homogenized and recompacted Ultisols, *Soil Tillage Res.*, *76*, 125–137, doi:10.1016/j.still.2003.09.006.

Poulsen, T. G., P. Moldrup, B. V. Iversen, and O. H. Jacobsen (2002), Three-region Campbell model for unsaturated hydraulic conductivity in undisturbed soils, *Soil Sci. Soc. Am. J.*, *66*, 744–752.

Press, W. H., B. P. Flannery, S. A. Teukolsky, and W. T. Vetterling (Eds.) (1986), Evaluation of functions, in *Numerical Recipes: The Art of Scientific Computing*, pp. 145–146, Cambridge Univ. Press, New York.

Richard, G., I. Cousin, J. F. Sillon, A. Bruand, and J. Guerif (2001), Effect of compaction on the porosity of a silty soil: Influence on unsaturated hydraulic properties, *Eur. J. Soil Sci.*, *52*, 49–58, doi:10.1046/j.1365-2389.2001.00357.x.

Schaap, M. G., and M. T. van Genuchten (2005), A modified Mualem-van Genuchten formulation for improved description of the hydraulic conductivity near saturation, *Vadose Zone J.*, *5*, 27–34, doi:10.2136/vzj2005.0005.

Schaffer, B., T. L. Mueller, M. Stauber, R. Muller, M. Keller, and R. Schulin (2008), Soil and macro-pores under uniaxial compression. II. Morphometric analysis of macro-pore stability in undisturbed and repacked soil, *Geoderma*, *146*, 175–182, doi:10.1016/j.geoderma.2008.05.020.

Stange, C. F., and R. Horn (2005), Modeling the soil water retention curve for conditions of variable porosity, *Vadose Zone J.*, *4*, 602–613, doi:10.2136/vzj2004.0150.

Tarawally, M. A., H. Medina, M. E. Frometa, and C. A. Itza (2004), Field compaction at different soil-water status: Effects on pore size distribution and soil water characteristics of a Rhodic Ferralsol in western Cuba, *Soil Tillage Res.*, *76*, 95–103, doi:10.1016/j.still.2003.09.003.

van Dijke, M. I. J., and M. Piri (2007), Introduction to special section on Modeling of Pore-Scale Processes, *Water Resour. Res.*, *43*, W12S01, doi:10.1029/2007WR006332.

van Genuchten, M. T. (1980), A closed-form equation for predicting the hydraulic conductivity of unsaturated soils, *Soil Sci. Soc. Am. J.*, *44*, 892–898.

Zhang, S. L., H. Grip, and L. Lovdahl (2006), Effect of soil compaction on hydraulic properties of two loess soils in China, *Soil Tillage Res.*, *90*, 117–125, doi:10.1016/j.still.2005.08.012.

N. R. A. Bird, A. S. Gregory, and W. R. Whalley, Department of Soil Science, Rothamsted Research, Harpenden AL5 2JQ, UK.

G. M. Laudone and G. P. Matthews, School of Geography, Earth and Environmental Sciences, University of Plymouth, Devon PL4 8AA, UK. (pmatthews@plymouth.ac.uk)

A. G. de G. Matthews, Cavendish Laboratory, University of Cambridge, J. J. Thomson Avenue, Cambridge CB3 0HE, UK.